Rapid low-cost assembly of modular microvessel-on-a-chip with benchtop xurography

Shashwat S. Agarwal [1,*], Marcos Cortes-Medina [2,*], Jacob C. Holter [2,*], Alex Avendano [2], Joseph W. Tinapple [2], Joseph M. Barlage [4], Miles M. Menyhert [3], Lotanna M. Onua [3], Jonathan W. Song [1,5,†]

1: Department of Mechanical and Aerospace Engineering, The Ohio State University, Columbus OH 43210
2: Department of Biomedical Engineering, The Ohio State University, Columbus OH 43210
3: Department of Chemical and Biomolecular Engineering, The Ohio State University, Columbus OH 43210
4: Department of Biomedical Education and Anatomy, The Ohio State University, Columbus OH 43210
5: The Comprehensive Cancer Center, The Ohio State University, Columbus OH 43210

*Contributed equally
†Correspondence to: song.1069@osu.edu

Abstract

Blood and lymphatic vessels in the body are central to molecular and cellular transport, tissue repair, and pathophysiology. Several approaches have been employed for engineering microfabricated blood and lymphatic vessels *in vitro*, yet these approaches invariably require specialized equipment, facilities, and research training beyond the capabilities of most biomedical laboratories. Here we present xurography as an inexpensive, accessible, and versatile rapid prototyping technique for engineering cylindrical and lumenized microvessels. Using a benchtop xurographer, or a cutting plotter, we fabricated modular multi-layer poly(dimethysiloxane) (PDMS) -based microphysiological systems (MPS) that house endothelial-lined microvessels approximately 260μm in diameter embedded within a user-defined 3-D extracellular matrix (ECM). We validated the vascularized MPS (or vessel-on-a-chip) by quantifying changes in blood vessel permeability due to the pro-angiogenic chemokine CXCL12. Moreover, we demonstrated the reconfigurable versatility of this approach by engineering three different vessel-ECM arrangements, which were obtained by minor adjustments to one or two steps of the fabrication process. Several of these arrangements, such as ones that incorporate close-ended vessel structures and spatially distinct ECM compartments along the same microvessel, cannot be readily achieved with other microfabrication strategies. Therefore, we anticipate that our low-cost and easy-to-implement fabrication approach will facilitate wider accessibility of MPS with tunable vascular architectures and ECM components while reducing the turnaround time required for iterative designs.

Keywords: Microscale tissue engineering, vessel permeability, vascularized microphysiological systems, multi-layer microfabrication

Competing Financial Interests: Jonathan W. Song is a co-founder of and shareholder in EMBioSys, Inc.

1. Introduction

The microcirculation contains perfusable networks that are entangled, complex, and traditionally difficult to recreate and investigate their function *in vitro*.[1,2] These challenges have helped propel the use of microsystems engineering techniques, such as micropatterning based on PDMS,[1, 3, 4] stereolithography,[5, 6] extrusion 3-D printing,[7] and machine milling, for reproducing vascular geometry and structures *in vitro*.[8] In the context of "vessel-on-a-chip" technology, or vascularized microphysiological systems (MPS), these microsystem engineering techniques all serve the same fabrication goal of encapsulating endothelialized vessels within a platform that can: 1) recreate the complex geometry and function of blood and lymphatic vessels of the microcirculation, 2) allow for biological mechanism study, and 3) enable facile experimental manipulation and analysis.[9, 10]

Vessel-on-a-chip systems are recognized as important research tools as they have greatly contributed to advancing our understanding of the role of fluid forces,[4,11] extracellular matrix (ECM) composition,[12] stiffness,[13] and pathological conditions[14] in regulating vascular function. However, the adoption of vessel-on-a-chip systems among biologists and physiologists as well as other researchers with no prior microfabrication training still remains limited.[15] A major constraint is the established microsystems engineering processes that underlie the fabrication of MPS, which typically require considerable expertise and specialized equipment beyond the reach of most biomedical research labs.[16] For instance, a mainstay for microsystems engineering is patterning micron-scale features using photolithography and subsequent PDMS soft lithography of microfluidic devices.[17] However, photolithography requires dedicated cleanroom facilities that are not present or readily accessible at many research institutions. Moreover, PDMS soft lithography produces microchannels that have rectangular cross-sections unlike the circular cross sections or tubular structures that are characteristic of blood or lymphatic vessels *in vivo*. As reported by Vo et al.,[18] non-circular cross sections are accompanied by inhomogeneous interactions between cells and the adjacent ECM with a non-uniform distribution of shear stress. Several microfabrication techniques have been developed to generate vessels-on-a-chip with cylindrical-based channels encased in an ECM compartment within microfluidic systems.[19,20,21,22,23] Among these, techniques that use steel needles[24] or PDMS rods[22] to cast open lumens are widely used. After hydrogel polymerization, the rod or needle template is carefully removed using tweezers leaving behind a hollow cylindrical lumen. These lumens are then seeded with endothelial cells to form patent

engineered microvessels of a defined diameter such that the cell-cell and cell-ECM interactions are homogenous. However, fabrication of cylindrical vessels-on-a-chip most often requires soft lithography for positioning and templating of the needle or rod within a PDMS microdevice, which limits accessibility. Moreover, photolithography of silicon masters includes several complicated and potentially time-consuming steps, including the design and production of photomasks, which slows the turnaround time for design iterations.

Recently, xurography, or the use of razor printing using cutting plotters, has increased in popularity as this technique enables cost-efficient rapid prototyping and assembly of microfluidic devices.[25,26,27] Typically, xurography involves cutting a polymer sheet with micro-scale precision that is then bonded to other layers or adhesives to form relevant geometries, orientations, and compartmentalization critical for *in vitro* biomimicry of *in vivo* biology and physiology. Importantly, the main capital cost for xurography is a desktop cutting plotter and blades, which can be obtained for <$1,000 and readily deployed on the benchtops of standard wetlabs.[28] While xurography has grown in prominence as a method for fabrication of microfluidic devices due to its simplicity and ability to easily integrate multiple materials,[29] the majority of xurography-based microdevices have focused on biochemical applications and has not yet been extensively demonstrated and characterized for cell-culture applications, especially for 3-D organotypic cultures.[25] To our knowledge xurography-based fabrication has not been used for engineering vessel-on-a-chip systems with cylindrical microvessels.

To increase the availability of microfluidic devices to researchers that have limited experience in advanced fabrication techniques, we present xurography as an approach to engineer vascularized MPS containing cylindrical microvessels. We developed and validated our model by quantifying the vascular permeability of the endothelialized lumen in the presence and absence of a pro-angiogenic molecule, CXCL12. We demonstrate the ease and robustness of this modular approach for iterative designs by demonstrating four different vessel-on-a-chip configurations obtained through discrete modifications to only few of the steps in the fabrication process: 1) single open lumen vessel ("single vessel"); 2) single open lumen perpendicular to a close-ended lumen vessel ("T-shaped vessels"); 3) double opposing close-ended lumen vessel ("opposing vessels"); and 4) single open lumen vessel with multiple distinct ECM regions ("single vessel-multiple ECM regions"). We anticipate that our modular fabrication approach to engineer several distinct vessel-

on-a-chip configurations with desktop xurography will enable faster and more cost-efficient design iterations of vascularized MPS and increase accessibility and adoption of these 3-D culture models in biomedical laboratories.

2. Materials and Methods

2.1. <u>Cell Culture</u>

Commercially available human umbilical vascular endothelial cells (HUVECs, Lonza) and human dermal lymphatic endothelial cells (HDLECs, PromoCell) were purchased and maintained using endothelial cell growth medium-2 (EGM-2, Lonza, CC-3162) and EGM-2 MV (Lonza, CC-3202), respectively. Cell passage numbers of 5–10 were used in this study. Cells were cultured in a humidified incubator at 37°C and 5% CO_2 with media exchange every 2 days. Cells were collected for vessel-on-a-chip studies by first washing with 1X Dulbecco's phosphate-buffered saline (PBS) without Mg/Ca (1X DPBS, Gibco, 14190250) followed by detachment using 0.05% Trypsin-EDTA 1X (Gibco, 25300054) for 3-4 minutes to harvest the cells from the T-75 cell culture flasks. After neutralizing trypsin with 10% FBS in DMEM, HUVECs and HDLECs were resuspended in their respective media at a concentration of $10–50 \times 10^3$ cells/ul in preparation for seeding the lumens of the microfluidic devices.

2.2. <u>Poly(dopamine) coating of PDMS surfaces</u>

Poly(dopamine) (PDA) is a mussel-inspired multifunctional material that has been shown to enhance surface anchorage of ECM hydrogels to PDMS surfaces.[30] To this end, 1 mg/ml PDA solution was prepared by mixing dopamine hydrochloride (Sigma-Aldrich, H8502) with 10mM, pH 8.5 tris-HCl buffer (Bioworld, 420204141). To prevent contamination, PDA solution was filtered through a 0.22-µm pore size PES syringe filter. 15 µl of PDA solution was injected in each device through the side gel port–enough to completely fill the gel chamber—and the devices were incubated for 1 hour at room temperature or 37 °C. Subsequently, the PDA solution was aspirated from the ECM chamber followed by rigorously rinsing the ECM chamber with 1X PBS three times. To ensure proper washing, 15 µl of 1X PBS was injected through the side port swishing 10 times via pipette. After washing, the devices were placed in 100 mm culture dishes, wrapped in parafilm, and stored overnight in the incubator at 37 °C.

2.3. <u>Preparation of collagen-based matrices</u>

Polymerized type I collagen (Corning, 354249) matrices were prepared per manufacturer's instructions. Briefly, rat-tail type I collagen (henceforth referred to simply as "collagen") stored in acidic solution was neutralized to pH = 7.4 using sodium hydroxide in 10X phosphate-buffered saline. Sterilized water was then utilized to adjust the final concentration of collagen to 6 mg/ml. Collagen gels were preincubated at 4 °C for approximately 12 min prior to casting to enhance fiber formation.[31] Upon neutralization and preincubation, collagen gels were pipetted into the ECM region of the microvessel-on-chip system and allowed to polymerize for 30 minutes.

2.4. <u>Microvessel-on-chip assembly using xurography</u>

The assembly for the microvessel-on-chip consists of the following components: a) a single 400-μm PDMS sheet, b) three 250-μm PDMS sheets, c) a single glass slide and d) a ~260-μm diameter PDMS rod (Figure 1A, Supplementary Video 1). This assembly permitted the specification of a cell inlet and outlet port, a PDMS rod connecting these ports, and a central region housing the ECM. The 400-μm and 250-μm thick PDMS sheets were formed by spin coating (Specialty Coating Systems, 6812P) on silanized 10-cm diameter silicon wafers at 115 rpm and 170 rpm, respectively. The PDMS coated wafers were cured for at least 4 hours up to overnight in a 65 ºC oven. Subsequently, the PDMS layers were peeled away from the wafer and cut into 7.5 cm x 4 cm rectangular sheets.

A desktop and computer-controlled cutting plotter (Graphtec, CE7000) was used to etch an 8-mm-long and 800-μm-wide rectangular channel in the 400-μm PDMS layer (henceforth called the "channel layer"), with a plugin for Adobe Illustrator (Graphtec, Cutting Master Version 5). The channel layer was irreversibly bonded to one of the 250-μm sheets (henceforth referred to as "membrane layer 1") using plasma oxidation (Harrick Plasma, PDC-32G). A second membrane layer (membrane layer 2) was used and registered with the two-layer assembly. 1.5-mm and 4-mm diameter biopsy punches were used to create the inlet and outlet ports, respectively. Biopsy punches cored through the three layers and membrane layer 2 was peeled away and set aside for a later step. Subsequently, a third membrane layer ("membrane layer 3") was irreversibly sealed to the channel layer with plasma oxidation. Thus, the three-layer assembly consisted of the channel layer sandwiched by membrane layer 1 and membrane layer 3. In between and equidistant to the

inlet and outlet ports, a 4 mm biopsy punch was used to core through all three layers to form the ECM chamber. Finally, the previously punched membrane layer 2 was irreversibly plasma bonded against membrane layer 1 to yield a four-layer PDMS device assembly. Plasma bonding was aided by spraying 70% ethanol on the PDMS layers, which facilitated alignment of layers during device assembly. The final assembly step was using 1.5-mm biopsy punches to core side ports on the periphery of the ECM chamber for gel loading. Afterwards, a ~260-µm diameter PDMS rod was inserted in the microchannel layer from the inlet port through to the outlet port. The rod was suspended between membrane layers 1 and 3. PDMS rods were created by loading needles (BD, Precision Glide 25G) with PDMS and cured for at least 30 minutes. The PDMS rods were retrieved by breaking the needles with pliers, pulling with tweezers, and trimming the rod to the desired length. The devices were then irreversibly bonded to glass slides. The final assembly was sterilized with UV for 30 minutes.

The ECM chamber was coated with 1 mg/ml PDA solution, incubated for 1 hour, rinsed with 1X PBS thrice and stored at 37 °C overnight. Subsequently, collagen-based solutions were added in the ECM chamber. After collagen gelation, the PDMS rod was removed using tweezers, leaving a hollow ductal lumen structure ~260-µm in diameter (Figure 1B). Before proceeding to cell seeding, the lumen was coated with 100 µg/ml fibronectin for at least 30 minutes and then flushed with cell culture media. Subsequently, 2 µl of HUVECs suspended at 50,000 cells/ul were seeded into the lumen to form an intact microvessel. Following this, the devices were rotated by placing upside down for 30 minutes, followed by 15-minute intervals on each side, and 20 minutes oriented normally. Afterwards, culture media was added to flush the devices, eliminating any extraneous suspended cells or cellular debris. Media was exchanged daily for all conditions. For devices treated with CXCL12-α, 100 ng/ml of the chemokine containing cell culture media was introduced inside the microvessel 1 day after seeding.

2.5. <u>Microfluidic vessel permeability measurement</u>

Apparent vessel permeability measurements were made on Day 3 by passively pumping 20 kDa Fluorescein isothiocyanate (FITC)-Dextran added to HUVEC culture media (10 µM) into the cell-lined lumen. The change in intensity as the fluorescent dye diffused across the entire vessel lumen was tracked by using time-lapse microscopy. Images were recorded every 5 s for a total of 5 minutes using a Nikon TS-100F microscope equipped with a Q-Imaging QIClick camera

controlled with the NIS-Elements software. A custom MATLAB algorithm was then developed to automatically estimate the vessel permeability from the time-lapse movies. The script tracks the changes in fluorescent intensity and estimates the vascular permeability by assuming a linear increase in the intensity as the FITC-Dextran extravasates to the surrounding ECM by diffusion. Permeability was measured as:

$$P = \frac{1}{I_0} \times \frac{dI}{dt} \times \frac{r}{2},$$

Where dI/dt describes the change of intensity as the dye permeates, I_0 equals the instantaneous increase in intensity when the solute is introduced, and r is the radius of the vessel (assuming a cylindrical shape).[32]

2.6. <u>Fluorescence Microscopy</u>

We used methods to successfully stain the cells of blood and lymphatic microvessels in collagen hydrogels within our MPS.[33] Briefly, at Day 3, cells of microvessels were fixed with 4% paraformaldehyde (PFA) for 30 min at room temperature (RT), permeabilized with 0.2% Triton X-100 for 30 min at RT, blocked with Blocking Buffer for 30 min at RT, and subsequently stained for either nuclei (DAPI, Sigma-Aldrich, D9542), VE-cadherin (monoclonal antibody, BD Biosciences, 561567), or F-actin (phalloidin, Fisher Scientific, A12379). Microvessels were washed three times between each step with Washing Buffer: 0.1% Tween 20 in 1X PBS. Blocking Buffer consisted of 1% BSA in Washing Buffer. VE-cadherin was stained overnight at 4°C, phalloidin was stained for 60 min at RT, and lastly DAPI was counterstained for 10 min. Images were taken using a Nikon A1R Live Cell Imaging Confocal Microscope controlled with NIS-Elements Software. The same microscope was used for visualization of collagen fibers with confocal reflectance microscopy, which is an imaging modality that requires no staining.[34] We used reflectance microscopy techniques previously described by our group.[35]

2.7. <u>Statistical Analysis</u>

Statistical analysis was conducted using Student's t-test. All results shown are presented with error bars representing the standard error of the mean (SEM). Each experimental condition was run with

at least 4 biological replicates for statistical evaluation. A p-value of 0.05 was used as a threshold for statistical significance.

3. Results and Discussion

3.1 Xurography enabled fabrication of an endothelialized single open lumen microvessel

Figure 1A shows detailed or "IKEA-like" assembly instructions for fabricating a single vessel-on-a-chip model, further visualized by Supplementary Video 1. We used a PDMS rod of diameter 260-μm to obtain the cylindrical structure, as shown in Figure 1B. Notably, the entire fabrication process requires a spin-coater, a low-cost benchtop plotter, biopsy punches and a plasma oxidizer, all of which do not require a cleanroom facility. We confirmed the barrier integrity and circular cross-section of the endothelialized microvessel through staining of VE-cadherin and nuclei as shown in Figure 1C, D. Subsequently, the barrier function of the vessel-on-a-chip model was validated by assessing the extravasation of a fluorescent molecule (20 kDa FITC-Dextran) across the vessel wall and into the ECM in the presence and absence of CXCL12, as shown in Figure 1E, F. The single vessel was subjected to EGM-2 media supplemented with 100 ng/ml CXCL12 and EGM-2 alone as control for 3 days. CXCL12 exists as several isoforms, is secreted by cancer-associated fibroblasts (CAFs), and is known to stimulate cancer growth and intravasation, as well as regulate vessel permeability through paracrine signaling.[3,36,37] We have also previously shown that CXCL12 mediates blood vessel sprouting and permeability in a microvessel analogue.[3, 38] As shown in Figure 1G, microvessels exposed to the alpha isoform of CXCL12 (CXCL12-α) demonstrated a statistically significant increase in permeability compared to control conditions. While determining vessel responses to CXCL12 is not novel,[3, 38] the validation of the assay promotes the feasibility to further interrogate the endothelial lumen with other angiogenic agents, most notably vascular endothelial growth factor (VEGF), or with molecular therapies serving to combat angiogenesis.

3.2 Engineered T-shaped and opposing close-ended vessel configurations

Next, we demonstrated the modularity of our xurography fabricated vessels-on-a-chip technique by incorporating closed or blind ended vessels to the vascular arrangements. Current strategies for templating straight cylindrical vessels typically require the lumen structure to be both continuous

and open to both the inlet and outlet. One such example is viscous finger patterning where a continuous tubular lumen structure is formed along a single microchannel by displacing viscous ECM gel with less viscous fluid without needing to insert an external mold.[39] Moreover, several vessel-on-a-chip systems have templated multiple open lumen vessels.[40] These vessels are typically arranged in parallel to each other. However, closed-, or blind-ended vessels are also present in physiological vascular systems. The microanatomy of closed or blind ended vessels are typically attributed to initial lymphatics (or lymphatic capillaries).[41] Yet, closed vessels also occur in the blood microcirculation, such as during wound repair and prior to successful tissue restoration.[42]

A close-ended microvessel was engineered using xurography by modifying the placement of the cylindrical template used in the fabrication process, such that one end of the template is located within the ECM chamber. To achieve this microanatomy, either a PDMS rod or nitinol wire (both ~260μm in diameter) can be used as a template. Unlike the single open vessel configuration where the cylindrical template can be secured or anchored at two opposing ends (Figure 1A, step 9), the cylindrical template for a close-ended vessel is secured only at one end (Figure 2A, Supplementary Figure 1, step 9). Thus, one of the benefits of using the nitinol wire for a close-ended vessel is that its rigidity facilitates its stable placement as a cylindrical template while the unsecured end is suspended in the ECM gel (Supplementary Figure 1, step 11). Moreover, unlike that of PDMS rods which need to be recovered manually with tweezers, nitinol wires can be removed post gelation of collagen with a vacuum aspirator.

We fabricated endothelialized "T-shaped vessels" by incorporating an open lumen perpendicular to a close-ended lumen (Figure 2A). To achieve this configuration, as shown in Supplementary Figure 1, step 2 is modified to cut two perpendicular channels instead of a single channel and a second 1.5mm biopsy punch is cored in step 4. In addition, a PDMS rod and a nitinol wire were added and removed in steps 9 and 12, respectively, to obtain the microvessels. As shown in Figure 2B, this vessel-on-a-chip model affords the capability to control the inter-vessel distance (i.e., the distance between the close-ended and the open microvessels, δ). An important design feature due to the xurography fabrication process is that the PDMS rod and nitinol wire are placed on the same layer (step 9 in Supplementary Figure 1). This arrangement ensures that the resultant open vessel and closed vessel of the T-shape are in plane with each other, which is crucial for concurrent

imaging of both vessel structures with high resolution 3D imaging (e.g., laser scanning confocal microscopy).

Similarly, we used the close-ended vessel fabrication technique to engineer two opposing vessels or double close-ended lumen vessels as shown in Figure 3A. To achieve this arrangement, two 260-μm diameter nitinol wires were added from opposite ports in step 10 of the multi-step fabrication process (Supplementary Figure 2A). The rigidity of the nitinol wire affords the capability to control the distance (δ) between the two close-ended lumens, which were seeded with HDLECs. This configuration mimics two opposing blind-ended capillary lymphatics, which can be used to probe vascular dynamics and crosstalk between these structures. Since the two vessels are in the same layer of the multi-layer PDMS device, they are on the same imaging plane and amenable to concurrent imaging with confocal microscopy (Supplementary Figure 2B).

3.3 Engineered single open lumen vessel with multiple distinct ECM regions

In addition to modifying the vascular arrangements, our xurography fabricated microvessel construct is amenable to spatially distinct ECM compartments along the same open vessel lumen (Figure 4 A, B). The "single vessel-multiple ECM regions" configuration models heterogeneous tissue environments by specifying two distinct ECM compositions. One approach for conferring heterogeneous environments along a single microvessel-like structure was shown previously using a multi-layer membrane microdevice.[43] However, one challenge, especially for those without microsystems engineering training, is that membrane microdevices often require several PDMS stamping and bonding steps to ensure proper sealing of layers.[44, 45] Moreover, the membranes used for these microdevices are flat, which restricts the endothelia integrated in these microdevices to be planar (i.e., non-circular cross-section). The single vessel-multiple ECM regions arrangement presented here was created by a simple modification to the fabrication of a single open vessel (Figure 1A). As shown in Supplementary Figure 3, two localized ECM environments were obtained by punching two 2-mm biopsy punches in step 6 rather than using one single 4-mm biopsy punch. Figure 4B shows two distinct localized ECM chambers containing 3 mg/ml and 6 mg/ml collagen embedded with fluorescent microspheres of different colors. The viscosity of the pre-polymerized ECM gel imparts the ability to control the space that is filled by the ECM being injected. Moreover, the sequence of ECM injection plays a crucial role in minimizing overflow of pre-polymerized ECM gel to the neighboring ECM chamber. The 6 mg/ml collagen pre-polymer

was injected first since this gel is denser and more viscous than the 3 mg/ml collagen (Figure 4B). This stepwise procedure ensures the formation of a distinct boundary between the two ECM chambers.

The xurography fabrication process also affords the ability to modify the length of the razor cut in step 2 (Supplementary Figure 3). While we show two distinct and localized ECM chambers, we envision that more than two of these chambers can be readily incorporated by extending the length of the microvessel and biopsy punching multiple ECM chambers (Supplementary Figure 3, Step 6). Each of these chambers can be used to generate organ- or tissue-specific microenvironments conferred by non-cellular (e.g., ECM proteins) and cellular (e.g., stromal fibroblasts) components encapsulated within the ECM chambers along a single microvessel.[38] Such capabilities would be beneficial to organs-on-a-chip and/or body-on-a-chip studies, which need to mimic ECM environments of several organs on a single MPS. The multiple ECM configuration can also be reconfigured to change the sizes of the ECM chambers and specify the order in which they are perfused. Both size and compartmental arrangement have been attributed to be of great importance in organs-on-a-chip systems.[46]

4. Summary and Conclusions

Xurography-based approaches have enabled researchers to fabricate microfluidic devices and MPS made from PDMS without the need for cleanroom facilities and lithographic expertise. Thus, xurography has emerged as an attractive and cost-effective rapid prototyping method with pathways for automated batch processing of microdevices.[25] The mechanical properties of PDMS are well-suited for cutting plotter machines to pattern and cut distinct geometries for assembly of multi-layer devices. Hence, these devices retain the positive attributes of PDMS, such as optical transparency, biocompatibility, and gas permeability. In this proof-of-concept work, we report a novel implementation of xurography-based fabrication in the engineering of a modular vessel-on-a-chip system. We demonstrate the robustness of the modular approach by fabricating four distinct configurations of the vessel-on-a-chip model, which were obtained by simply modulating one or a few fabrication steps. We believe that several of these configurations are novel geometries (e.g., T-shaped vessels, opposing close-ended vessels, and single vessel with multiple ECM regions) for the xurography approach.

Our fabrication process has high throughput and enables batch production, with batches consisting of up to 20 devices containing cylindrical microvessels. A typical turnaround time for one batch of 20 devices is ~7 hours prior to the hydrogel step (see Supplementary Table 1). This time can be subdivided into "work time" (~2 hours) and "wait time" (~5 hours). In this sense, 20 open lumen devices can be made in approximately 2 hours of labor, which results in a rate of about 6 minutes of labor per device. Furthermore, inter-batch steps can be performed in parallel during wait times to significantly increase throughput. Additionally, total turnaround time can be further optimized: "wait time" can be decreased by increasing the curing temperature and reducing curing time of the spin coated PDMS layers.[47] For instance, Kwak et al. reduced the curing time of PDMS from 4 hours to 2 hours by increasing the curing temperature from 65 ºC to 80 ºC.[48] Alternatively, prefabricated PDMS sheets can be acquired from several commercial vendors worldwide (e.g., SiMPore, DiagnoCine, etc.), thereby eliminating the PDMS spin coating step from the workflow.

In addition to reducing the cost and increasing accessibility of vessel-on-a-chip systems for researchers with limited microsystems engineering expertise, we foresee that the xurography-based fabrication techniques presented in this paper will augment current research workflows. During any research project, new questions of interest unfailingly arise, which prompt requests for new microfabricated designs with unique geometries and capabilities. With soft lithography/photolithography-based approaches, a new microfabricated design would require acquisition of a photomask and production of new silicon masters. This process requires many intricate steps with several potential bottlenecks. These bottlenecks may include external factors that are beyond the researcher's control, such as disruptions in reagent supply chains and restricted access to specialized facilities, such as cleanrooms. Both obstacles were heightened to unprecedented levels during the COVID-19 pandemic. Here we replicate a workflow of microvessel designs with increasing complexity, ranging from a single vessel, T-shaped vessels, opposing vessels, and single vessel-multiple ECM regions. Importantly, all the fabrication steps can be conducted in-house within the same laboratory without reliance on external entities or specialized facilities. Thus, while the expected turnaround time for a new microfabricated design using established techniques can be on the order of >1 week, one can realistically expect a new design using xurography-based microfabrication conducted in-house within 1 day.

The relative ease of control for geometry of both the lumen and the microdevice due to xurography enables the addition of other factors like tumor cells, stromal cells, and perfusion resulting in shear stress and interstitial flow.[49] This work also builds upon previous research using templating methods for engineering lumen structures with opportunities to expand this technique. For instance, the PDMS rod templating approach augments the robustness as several PDMS rods can be joined to mimic bifurcated vessel configuration or engineering microvessels with a non-uniform diameter.[22] The latter can be achieved by bonding a higher diameter PDMS rod with a relatively smaller diameter PDMS rod. Furthermore, xurography can also enable microfabrication of parallel vessels by cutting two or more rectangles in the channel layer. Moreover, while our studies focused on engineered microvessels, many other tubular structures besides blood and lymphatic vessels exist in physiology, such as mammary ducts and kidney tubules. Several studies have emphasized the importance of 3-D lumen tissue geometry and spatial organization in mediating phenotypic behavior of several cell types,[50,51,52,53] such as cancer, endothelial, and kidney epithelial. Thus, our approach for microfabricated microvessels can be readily adapted for studying other tubular structures in physiologic-like environments, with improved accessibility for all researchers.

Acknowledgements

References

1.   Akbari E, Spychalski GB, Song JW. Microfluidic approaches to the study of angiogenesis and the microcirculation. Microcirculation. 2017;24(5). doi: 10.1111/micc.12363. PubMed PMID: 28182312.

2.   Kim S, Lee H, Chung M, Jeon NL. Engineering of functional, perfusable 3D microvascular networks on a chip. Lab Chip. 2013;13(8):1489-500. doi: 10.1039/c3lc41320a. PubMed PMID: 23440068.

3.   Chang CW, Seibel AJ, Avendano A, Cortes-Medina MG, Song JW. Distinguishing Specific CXCL12 Isoforms on Their Angiogenesis and Vascular Permeability Promoting Properties. Adv Healthc Mater. 2020;9(4):e1901399. Epub 20200115. doi: 10.1002/adhm.201901399. PubMed PMID: 31944591; PMCID: PMC7033017.

4.   Song JW, Munn LL. Fluid forces control endothelial sprouting. Proc Natl Acad Sci U S A. 2011;108(37):15342-7. Epub 20110829. doi: 10.1073/pnas.1105316108. PubMed PMID: 21876168; PMCID: PMC3174629.

5.   Grigoryan B, Paulsen SJ, Corbett DC, Sazer DW, Fortin CL, Zaita AJ, Greenfield PT, Calafat NJ, Gounley JP, Ta AH, Johansson F, Randles A, Rosenkrantz JE, Louis-Rosenberg JD, Galie PA, Stevens KR, Miller JS. Multivascular networks and functional intravascular topologies within biocompatible hydrogels. Science. 2019;364(6439):458-64. doi: doi:10.1126/science.aav9750.

6.   Wang WY, Lin D, Jarman EH, Polacheck WJ, Baker BM. Functional angiogenesis requires microenvironmental cues balancing endothelial cell migration and proliferation. Lab Chip. 2020;20(6):1153-66. doi: 10.1039/c9lc01170f. PubMed PMID: 32100769; PMCID: PMC7328820.

7.   Hauser PV, Chang HM, Nishikawa M, Kimura H, Yanagawa N, Hamon M. Bioprinting Scaffolds for Vascular Tissues and Tissue Vascularization. Bioengineering (Basel). 2021;8(11). Epub 20211106. doi: 10.3390/bioengineering8110178. PubMed PMID: 34821744; PMCID: PMC8615027.

8.   Wong JF, Mohan MD, Young EWK, Simmons CA. Integrated electrochemical measurement of endothelial permeability in a 3D hydrogel-based microfluidic vascular model. Biosens Bioelectron. 2020;147:111757. Epub 20191003. doi: 10.1016/j.bios.2019.111757. PubMed PMID: 31654819.

9.   Fleischer S, Tavakol DN, Vunjak-Novakovic G. From Arteries to Capillaries: Approaches to Engineering Human Vasculature. Advanced Functional Materials. 2020;30(37):1910811. doi: https://doi.org/10.1002/adfm.201910811.

10.   Moses SR, Adorno JJ, Palmer AF, Song JW. Vessel-on-a-chip models for studying microvascular physiology, transport, and function in vitro. American Journal of Physiology-Cell Physiology. 2021;320(1):C92-C105. doi: 10.1152/ajpcell.00355.2020. PubMed PMID: 33176110.

11.   Helm C-LE, Fleury ME, Zisch AH, Boschetti F, Swartz MA. Synergy between interstitial flow and VEGF directs capillary morphogenesis <i>in vitro</i> through a gradient amplification mechanism. Proceedings of the National Academy of Sciences. 2005;102(44):15779-84. doi: doi:10.1073/pnas.0503681102.

12.   Lugo-Cintron KM, Ayuso JM, White BR, Harari PM, Ponik SM, Beebe DJ, Gong MM, Virumbrales-Munoz M. Matrix density drives 3D organotypic lymphatic vessel activation in a

microfluidic model of the breast tumor microenvironment. Lab Chip. 2020;20(9):1586-600. Epub 20200416. doi: 10.1039/d0lc00099j. PubMed PMID: 32297896; PMCID: PMC7330815.

13.   Bordeleau F, Mason BN, Lollis EM, Mazzola M, Zanotelli MR, Somasegar S, Califano JP, Montague C, LaValley DJ, Huynh J, Mencia-Trinchant N, Negrón Abril YL, Hassane DC, Bonassar LJ, Butcher JT, Weiss RS, Reinhart-King CA. Matrix stiffening promotes a tumor vasculature phenotype. Proceedings of the National Academy of Sciences. 2017;114(3):492-7. doi: doi:10.1073/pnas.1613855114.

14.   Reid SE, Kay EJ, Neilson LJ, Henze AT, Serneels J, McGhee EJ, Dhayade S, Nixon C, Mackey JB, Santi A, Swaminathan K, Athineos D, Papalazarou V, Patella F, Roman-Fernandez A, ElMaghloob Y, Hernandez-Fernaud JR, Adams RH, Ismail S, Bryant DM, Salmeron-Sanchez M, Machesky LM, Carlin LM, Blyth K, Mazzone M, Zanivan S. Tumor matrix stiffness promotes metastatic cancer cell interaction with the endothelium. EMBO J. 2017;36(16):2373-89. Epub 20170710. doi: 10.15252/embj.201694912. PubMed PMID: 28694244; PMCID: PMC5556271.

15.   Hargrove-Grimes P, Low LA, Tagle DA. Microphysiological Systems: Stakeholder Challenges to Adoption in Drug Development. Cells Tissues Organs. 2022;211(3):269-81. Epub 20210811. doi: 10.1159/000517422. PubMed PMID: 34380142; PMCID: PMC8831652.

16.   Mansouri M, Lam J, Sung KE. Progress in developing microphysiological systems for biological product assessment. Lab Chip. 2024;24(5):1293-306. Epub 20240227. doi: 10.1039/d3lc00876b. PubMed PMID: 38230512.

17.   Qin D, Xia Y, Whitesides GM. Soft lithography for micro- and nanoscale patterning. Nat Protoc. 2010;5(3):491-502. Epub 20100218. doi: 10.1038/nprot.2009.234. PubMed PMID: 20203666.

18.   Vo Q, Carlson KA, Chiknas PM, Brocker CN, DaSilva L, Clark E, Park SK, Ajiboye AS, Wier EM, Benam KH. On-Chip Reconstitution of Uniformly Shear-Sensing 3D Matrix-Embedded Multicellular Blood Microvessel. Advanced Functional Materials. 2024;34(10):2304630. doi: https://doi.org/10.1002/adfm.202304630.

19.   Silvestri VL, Henriet E, Linville RM, Wong AD, Searson PC, Ewald AJ. A Tissue-Engineered 3D Microvessel Model Reveals the Dynamics of Mosaic Vessel Formation in Breast Cancer. Cancer Research. 2020;80(19):4288-301. doi: 10.1158/0008-5472.Can-19-1564.

20.   Partyka PP, Godsey GA, Galie JR, Kosciuk MC, Acharya NK, Nagele RG, Galie PA. Mechanical stress regulates transport in a compliant 3D model of the blood-brain barrier. Biomaterials. 2017;115:30-9. doi: https://doi.org/10.1016/j.biomaterials.2016.11.012.

21.   Bouhrira N, DeOre BJ, Sazer DW, Chiaradia Z, Miller JS, Galie PA. Disturbed flow disrupts the blood-brain barrier in a 3D bifurcation model. Biofabrication. 2020;12(2):025020. doi: 10.1088/1758-5090/ab5898.

22.   Jiménez-Torres JA, Peery SL, Sung KE, Beebe DJ. LumeNEXT: A Practical Method to Pattern Luminal Structures in ECM Gels. Advanced Healthcare Materials. 2016;5(2):198-204. doi: https://doi.org/10.1002/adhm.201500608.

23.   Yan L, Dwiggins CW, Gupta U, Stroka KM. A Rapid-Patterning 3D Vessel-on-Chip for Imaging and Quantitatively Analyzing Cell-Cell Junction Phenotypes. Bioengineering (Basel). 2023;10(9). Epub 20230913. doi: 10.3390/bioengineering10091080. PubMed PMID: 37760182; PMCID: PMC10525190.

24.   Chrobak KM, Potter DR, Tien J. Formation of perfused, functional microvascular tubes in vitro. Microvascular Research. 2006;71(3):185-96. doi: https://doi.org/10.1016/j.mvr.2006.02.005.

25.   Stallcop LE, Alvarez-Garcia YR, Reyes-Ramos AM, Ramos-Cruz KP, Morgan MM, Shi Y, Li L, Beebe DJ, Domenech M, Warrick JW. Razor-printed sticker microdevices for cell-based applications. Lab Chip. 2018;18(3):451-62. doi: 10.1039/c7lc00724h. PubMed PMID: 29318250; PMCID: PMC5821501.

26.   Liu J, Mahony JB, Selvaganapathy PR. Low-cost and versatile integration of microwire electrodes and optical waveguides into silicone elastomeric devices using modified xurographic methods. Microsystems & Nanoengineering. 2017;3(1):17040. doi: 10.1038/micronano.2017.40.

27.   Tran R, Hoesli CA, Moraes C. Accessible dynamic micropatterns in monolayer cultures via modified desktop xurography. Biofabrication. 2021;13(2):025003. doi: 10.1088/1758-5090/abce0b.

28.   Martinez-Lopez JI, Mojica M, Rodriguez CA, Siller HR. Xurography as a Rapid Fabrication Alternative for Point-of-Care Devices: Assessment of Passive Micromixers. Sensors (Basel). 2016;16(5). Epub 20160516. doi: 10.3390/s16050705. PubMed PMID: 27196904; PMCID: PMC4883396.

29.   Shahriari S, Patel V, Selvaganapathy PR. Xurography as a tool for fabrication of microfluidic devices. Journal of Micromechanics and Microengineering. 2023;33(8):083002. doi: 10.1088/1361-6439/ace05d.

30.   Park SE, Georgescu A, Oh JM, Kwon KW, Huh D. Polydopamine-Based Interfacial Engineering of Extracellular Matrix Hydrogels for the Construction and Long-Term Maintenance of Living Three-Dimensional Tissues. ACS Applied Materials & Interfaces. 2019;11(27):23919-25. doi: 10.1021/acsami.9b07912.

31.   Avendano A, Chang JJ, Cortes-Medina MG, Seibel AJ, Admasu BR, Boutelle CM, Bushman AR, Garg AA, DeShetler CM, Cole SL, Song JW. Integrated Biophysical Characterization of Fibrillar Collagen-Based Hydrogels. ACS Biomater Sci Eng. 2020;6(3):1408-17. Epub 20200205. doi: 10.1021/acsbiomaterials.9b01873. PubMed PMID: 32292818; PMCID: PMC7156078.

32.   Huxley VH, Curry FE, Adamson RH. Quantitative fluorescence microscopy on single capillaries: alpha-lactalbumin transport. American Journal of Physiology-Heart and Circulatory Physiology. 1987;252(1):H188-H97. doi: 10.1152/ajpheart.1987.252.1.H188.

33.   Song JW, Bazou D, Munn LL. Anastomosis of endothelial sprouts forms new vessels in a tissue analogue of angiogenesis. Integr Biol (Camb). 2012;4(8):857-62. Epub 20120606. doi: 10.1039/c2ib20061a. PubMed PMID: 22673771; PMCID: PMC3759296.

34.   Brightman AO, Rajwa Bp Fau - Sturgis JE, Sturgis Je Fau - McCallister ME, McCallister Me Fau - Robinson JP, Robinson Jp Fau - Voytik-Harbin SL, Voytik-Harbin SL. Time-lapse confocal reflection microscopy of collagen fibrillogenesis and extracellular matrix assembly in vitro(0006-3525 (Print)).

35.   Cortes-Medina M, Bushman AR, Beshay PE, Adorno JJ, Menyhert MM, Hildebrand RM, Agarwal SS, Avendano A, Friedman AK, Song JW. Chondroitin sulfate, dermatan sulfate, and hyaluronic acid differentially modify the biophysical properties of collagen-based hydrogels. Acta Biomaterialia. 2024;174:116-26. doi: https://doi.org/10.1016/j.actbio.2023.12.018.

36.   Ahirwar DK, Nasser MW, Ouseph MM, Elbaz M, Cuitino MC, Kladney RD, Varikuti S, Kaul K, Satoskar AR, Ramaswamy B, Zhang X, Ostrowski MC, Leone G, Ganju RK. Fibroblast-derived CXCL12 promotes breast cancer metastasis by facilitating tumor cell intravasation. Oncogene. 2018;37(32):4428-42. Epub 20180503. doi: 10.1038/s41388-018-0263-7. PubMed PMID: 29720724; PMCID: PMC7063845.

37.   Zhao S, Chang SL, Linderman JJ, Feng FY, Luker GD. A Comprehensive Analysis of CXCL12 Isoforms in Breast Cancer(1,2). Transl Oncol. 2014;7(3):429-38. Epub 20140513. doi: 10.1016/j.tranon.2014.04.001. PubMed PMID: 24836649; PMCID: PMC4145355.

38.   Holter JC, Chang CW, Avendano A, Garg AA, Verma AK, Charan M, Ahirwar DK, Ganju RK, Song JW. Fibroblast-derived CXCL12 increases vascular permeability in a 3-D microfluidic model independent of extracellular matrix contractility. Front Bioeng Biotechnol. 2022;10:888431. Epub 20220902. doi: 10.3389/fbioe.2022.888431. PubMed PMID: 36118583; PMCID: PMC9478647.

39.   Bischel LL, Lee SH, Beebe DJ. A practical method for patterning lumens through ECM hydrogels via viscous finger patterning. J Lab Autom. 2012;17(2):96-103. Epub 20120124. doi: 10.1177/2211068211426694. PubMed PMID: 22357560; PMCID: PMC3397721.

40.   Zhao N, Pessell AF, Zhu N, Searson PC. Tissue-Engineered Microvessels: A Review of Current Engineering Strategies and Applications. Advanced Healthcare Materials. 2024;n/a(n/a):2303419. doi: https://doi.org/10.1002/adhm.202303419.

41.   Schmid-Schonbein GW. Microlymphatics and lymph flow. Physiological Reviews. 1990;70(4):987-1028. doi: 10.1152/physrev.1990.70.4.987.

42.   Sweat RS, Stapor PC, Murfee WL. Relationships between lymphangiogenesis and angiogenesis during inflammation in rat mesentery microvascular networks. Lymphat Res Biol. 2012;10(4):198-207. doi: 10.1089/lrb.2012.0014. PubMed PMID: 23240958; PMCID: PMC3525890.

43.   Song JW, Cavnar SP, Walker AC, Luker KE, Gupta M, Tung YC, Luker GD, Takayama S. Microfluidic endothelium for studying the intravascular adhesion of metastatic breast cancer cells. PLoS One. 2009;4(6):e5756. Epub 20090601. doi: 10.1371/journal.pone.0005756. PubMed PMID: 19484126; PMCID: PMC2684591.

44.   Chueh B-h, Huh D, Kyrtsos CR, Houssin T, Futai N, Takayama S. Leakage-Free Bonding of Porous Membranes into Layered Microfluidic Array Systems. Analytical Chemistry. 2007;79(9):3504-8. doi: 10.1021/ac062118p.

45.   Huh D, Fujioka H Fau - Tung Y-C, Tung Yc Fau - Futai N, Futai N Fau - Paine R, 3rd, Paine R 3rd Fau - Grotberg JB, Grotberg Jb Fau - Takayama S, Takayama S. Acoustically detectable cellular-level lung injury induced by fluid mechanical stresses in microfluidic airway systems(1091-6490 (Electronic)).

46.   Ronaldson-Bouchard K, Vunjak-Novakovic G. Organs-on-a-Chip: A Fast Track for Engineered Human Tissues in Drug Development. Cell Stem Cell. 2018;22(3):310-24. doi: 10.1016/j.stem.2018.02.011. PubMed PMID: 29499151; PMCID: PMC5837068.

47.   Speller NC, Morbioli GG, Cato ME, Cantrell TP, Leydon EM, Schmidt BE, Stockton AM. Cutting edge microfluidics: Xurography and a microwave. Sensors and Actuators B: Chemical. 2019;291:250-6. doi: 10.1016/j.snb.2019.04.004.

48.   Kwak TJ, Lee E. In vitro modeling of solid tumor interactions with perfused blood vessels. Scientific Reports. 2020;10(1):20142. doi: 10.1038/s41598-020-77180-1.

49.   Young EWK. Cells, tissues, and organs on chips: challenges and opportunities for the cancer tumor microenvironment. Integrative Biology. 2013;5(9):1096-109. doi: 10.1039/C3IB40076J.

50.   Rayner SG, Phong KT, Xue J, Lih D, Shankland SJ, Kelly EJ, Himmelfarb J, Zheng Y. Reconstructing the Human Renal Vascular–Tubular Unit In Vitro. Advanced Healthcare Materials. 2018;7(23):1801120. doi: https://doi.org/10.1002/adhm.201801120.

51.   Virumbrales-Munoz M, Ayuso JM, Gong MM, Humayun M, Livingston MK, Lugo-Cintron KM, McMinn P, Alvarez-Garcia YR, Beebe DJ. Microfluidic lumen-based systems for advancing tubular organ modeling. Chem Soc Rev. 2020;49(17):6402-42. doi: 10.1039/d0cs00705f. PubMed PMID: 32760967; PMCID: PMC7521761.

52.   Tien J, Ghani U, Dance YW, Seibel AJ, Karakan MC, Ekinci KL, Nelson CM. Matrix Pore Size Governs Escape of Human Breast Cancer Cells from a Microtumor to an Empty Cavity. iScience. 2020;23(11):101673. Epub 20201014. doi: 10.1016/j.isci.2020.101673. PubMed PMID: 33163933; PMCID: PMC7599434.

53.   Tan ML, Jenkins-Johnston N, Huang S, Schutrum B, Vadhin S, Adhikari A, Williams RM, Zipfel WR, Lammerding J, Varner JD, Fischbach C. Endothelial cells metabolically regulate breast cancer invasion toward a microvessel. APL Bioengineering. 2023;7(4). doi: 10.1063/5.0171109.
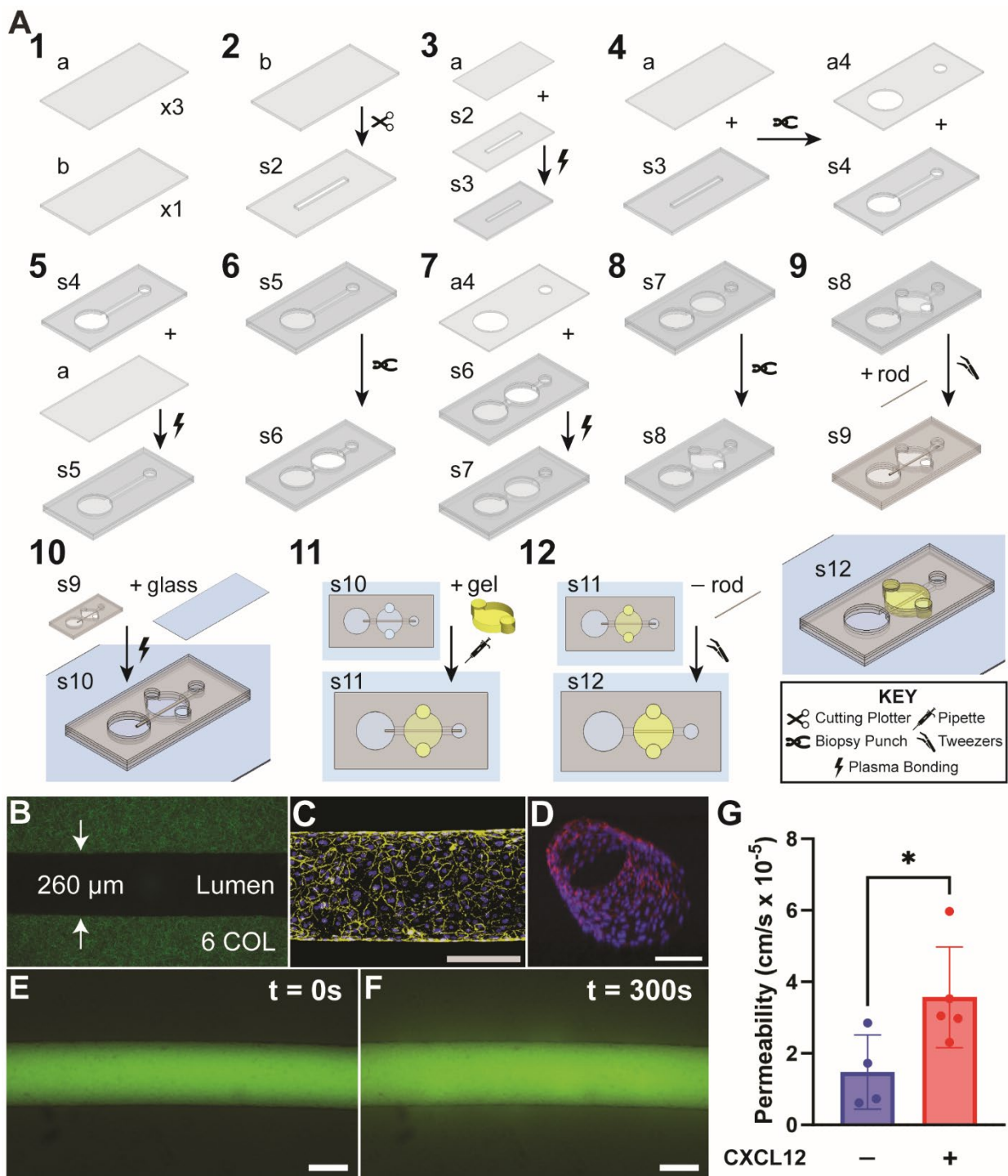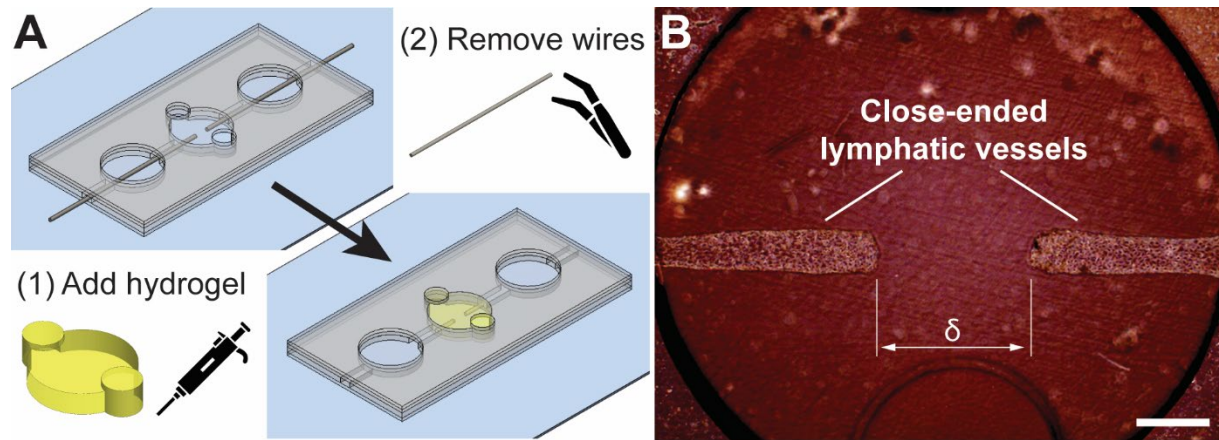
Figure 1: Engineered cylindrical microvessel model with benchtop xurography. A) Detailed and stepwise fabrication of the open lumen microdevice model. Step 1 begins with three 250-μm sheets (a) and one 400-μm sheet (b). This assembly permits the specification of an inlet and outlet port, a central hydrogel chamber, and a 260-um PDMS rod that stretches from port to port across the gel region. B) Confocal reflectance microscopy image of 6 mg/ml fibrillar type I collagen that is contained within the gel chamber of the model and encases an open lumen structure approximately 260μm in diameter. C) Confocal Z-projection of an intact cylindrical microvessel fully lined with HUVECs and stained for adherens junction protein VE-cadherin (monoclonal antibody, yellow) and nuclei counterstain (DAPI, blue). D) 3D render from confocal z-stack of cylindrical microvessel stained for F-actin (phalloidin, red) and nuclei (DAPI, blue). E) and F) Changes in fluorescent intensity tracer molecule (20-kDa FITC-conjugated Dextran), within the surrounding ECM that has been extravasated from the microvessel was used to calculate apparent vascular permeability after 5 minutes. G) Validation of the functionality of the microvessel by quantifying vessel permeability in the presence and

absence of 100 ng/mL CXCL12-α. CXCL12-α led to an increase in permeability of the HUVEC microvessel. Scale bars are 200 μm.
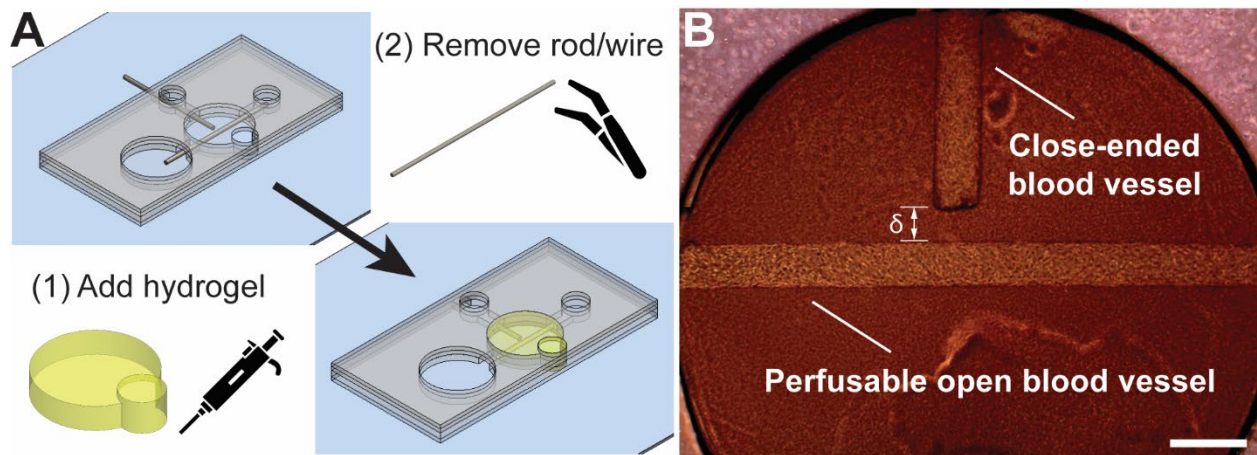
Figure 2: Engineered close-ended blood vessel oriented perpendicular to a perfusable open blood vessel. A) A PDMS rod and a nitinol wire are inserted from perpendicular directions, one of which is inserted near the center of the ECM chamber to constitute a terminated blood vessel. B) Phase contrast image of perpendicularly oriented microvessels fully lined with human umbilical vascular endothelial cells (HUVECs). The distance between the blind-end of the terminated vessel and the wall of the perfusable vessel (δ) can be specified based on the placement of the rod/wire. Scale bar is 500 μm.

Figure 3: Two engineered, opposing, close-ended microvessels lined with human dermal lymphatic endothelial cells (HDLECs). A) Two nitinol wires are inserted from opposite ends near the center of the ECM chamber to achieve the cylindrical close-ended structures. After wire removal, the back channel is plugged using liquid PDMS, which is subsequently cured once returned to the 37°C incubator. B) Phase contrast image of the double close-ended microvessels fully lined with HDLECs. The distance between the closed ends of the vessels (δ) can be specified based on the placement of the wires in A). Scale bar is 500 µm.
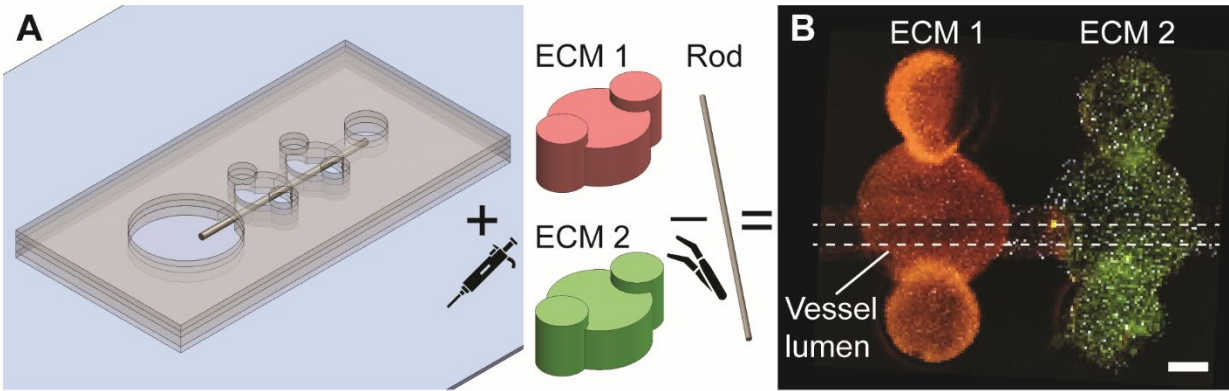
Figure 4: Engineered single open microvessel exposed to two distinct localized ECM microenvironments. A) The ECM localization is achieved by accommodating two separate central gel chambers and filling them with different hydrogels. After polymerization, the PDMS rod is removed to reveal the single lumen across both ECM compartments, which is then ready for seeding with endothelial cells. B) Fluorescent image of vessel-on-a-chip with distinct ECM environments, which are indicated by incorporating 1 μm fluorescent beads (red or green) prior to casting the two ECM gels. Scale bar is 500 μm.